Proceedings World Geothermal Congress 2026
Calgary, Canada, June 8 – 11, 2026

X-rays and thermal conductivity: towards 3D heat transfer modelling

Mathieu Des Roches[1, 2]*, Stéphanie Larmagnat[2], Jasmin Raymond[1], Christine Rivard[2], and Pierre Francus[1, 3]
Institut national de la recherche scientifique[1]*, Geological Survey of Canada, Natural Resources Canada[2], GEOTOP Research Centre[3]
mathieu.des_roches@inrs.ca

Keywords: CT-scan, X-ray imaging, thermal conductivity, heat transfer modelling

ABSTRACT

The performance of geothermal systems is highly dependent on rock properties. For deep (>1 km) open-loop systems, the critical reservoir properties to assess include porosity, permeability, and thermal conductivity (TC). The performance of closed-loop systems particularly depends on the rock TC. Various methods can be used to characterize the heterogeneous distribution of porosity and permeability at difference scales, but limited options are available for measuring TC. In situ heat injection tests made at the meter scale are hardly feasible in deep wells, and the divided bar method used with core plugs integrates heterogeneities at the centimeter scale. Infrared thermal conductivity scanner (TCS) measures variations of TC at the millimeter scale but is limited to 1D surface measurements that are not necessarily representative of the sample's internal structures. To overcome this issue, X-ray tomography (XCT) was used to produce 3D images of the sample's structure. The typical image resolution for a medical CT-scanner is in the sub-millimeter range. The level of X-ray attenuation mainly depends on three material characteristics: density, chemical composition, and porosity. The measurements obtained, in Hounsfield Unit (HU), combine these three properties, which are known to influence rock TC. To evaluate the correlation between the two types of analyses (XCT and TCS), a code was developed to accurately locate the two measurements on a set of sedimentary rock samples with different internal heterogeneities. This paper presents the algorithm developed to achieve the data alignment, the software interface for viewing the data and XCT unwrapped images, the correlation obtained (higher, R^2=0.9, for sandstone than limestone), and examples of 3D representation of TC. These results show that this approach appears promising for mapping the distribution of TC in 3D using X-ray imaging.

1 INTRODUCTION

Thermal conductivity (TC) is a material property that can be evaluated indirectly using different methods, generally involving the measurement of a sample temperature under a known heat flux. The need for fast, high-resolution sample characterisation has led to the development of instruments using transient methods. Popov et al. (1999) invented a Thermal Conductivity Scanner (TCS) that uses a moving infrared heat source that provides a 1D TC profile with a user-selectable sampling interval between 1 and 10 mm. Jorand et al. (2013) used a TCS to demonstrate how bedding plane orientation and scanning direction affected measurements, and how to overcome this. By scanning a sample in a grid-like pattern, a 2D TC map was produced and allowed the evaluation of TC anisotropy in two directions. Jorand et al. (2013) stated that the depth of investigation of the TCS, assumed to be 1 cm or less (Popov, 1997), "*limits the influence of internal heterogeneities on the TC measurement*" and therefore, does not allow a complete assessment of the material local anisotropy. More importantly, Jorand et al. (2013) demonstrated that mean TC is not equal to the effective TC obtained by numerical simulation of heat transfer mainly due to "*heterogeneous proportions of lateral heat flow within the sample*". The spatial organisation of the material must be taken into account for heterogeneous porous samples, emphasizing the limitation of 1D and 2D characterisation methods.

Directly measuring the temperature distribution inside a heated solid object is challenging, if not impractical. Therefore, we propose to explore the correlation between TC obtained with a TCS, and HU density obtained using X-ray computed tomography (XCT). Both material properties, TC and X-ray attenuation, depend on material composition, density and porosity. XCT provides a 3D representation of X-ray attenuation within a sample, offering a promising approach that could pave the way for 3D characterisation of TC, should a good correlation be found.

In order to compare TC and X-ray attenuation measurements, a code was developed to perform data registration and extract TCS and XCT values at the exact same location on a core-plug sample surface. This paper describes

the methodology and algorithm developed to carry out these operations, and presents the correlation obtained between the two properties.

2 METHODOLOGY

2.1 Sample set selection

A set of 30 core samples was used for this study. It includes 13 core samples from the Bécancour area in the province of Quebec (St. Lawrence Lowlands). Cores have a diameter of 38.1 mm (1.5 in) with lengths ranging from 30 to 67 mm. These samples were collected by different companies for oil and gas exploration and were used for various subsequent studies to evaluate the geothermal and CO_2 storage potential. These samples are sandstones collected at depths greater than 1 km, from the Cairnside and Coveyhill formations.

Seventeen so-called "reference" samples were obtained from Kocurek Industries, a Texas-based supplier specializing in high-quality reservoir cores sourced from various quarries across the United States. These reference samples are representative of known reservoir formations and are commonly used in both academic and industrial research. Alabama marble, Colton sandstone, Rocherons, Zebra, Torrey Buff, Parker, Winterset, Briarhill, Bentheimer, Desert Pink, Mount Gambier, and Edwards Brown were selected to cover a wide range of lithologies, mineral contents, TC and porosity.

2.2 Thermal conductivity profiles

A TCS has been used to acquire TC profiles along the surface of the samples. Their cylindrical shape limits the scanning direction parallel to the sample main axis, ruling out the investigation of TC anisotropy. The TCS uses a transient optical method where the heat flux, for each data point along the profile, is constrained to a plane perpendicular to the scanning direction. The measurement depth is considered 1 cm or less (Popov, 1997) and the scanning duration is in the order of a few seconds. A custom sample holder has been designed and 3D printed to position the lowest radial surface flush with the TCS top plate (Figure 1). Four scan lines were positioned and marked with a permanent marker at 90° intervals on the top surface (Figure 1). The samples were dried for 48 hours at 108 °C, then the radial surface was painted black using water-based paint, and left in the TCS room for at least 24 hours prior to the measurements to ensure that the internal temperature was homogeneous.

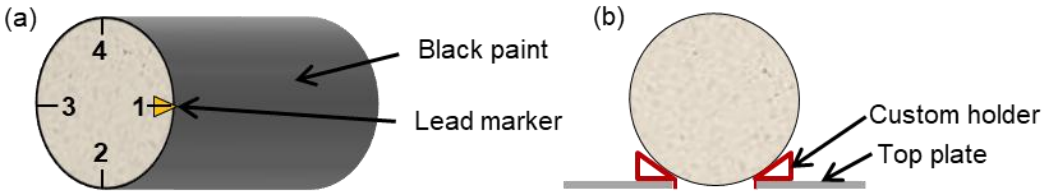


Figure 1 (a): position of scan lines and lead marker. (b): Custom support to hold the lower axial surface of the cylindrical sample flush with the instrument top plate

The measurement interval was set to 1 mm. For each profile, the user removes data at both ends to remove edge effects that are in the order of 1 cm. The scan lines #1 and #3 were performed first, then the sample was left at rest for at least five minutes to allow the internal temperature to stabilize. Next, scan lines #2 and #4 were completed, followed by another rest time of at least five minutes. This sequence was repeated three times, and the resulting three profiles for each scan line position were averaged together.

2.3 X-ray CT imaging and main sample features

X-ray imaging is achieved in two phases. First, the sample is irradiated by an X-ray beam with an I_0 intensity. Then, the beam is attenuated by the specimen, and the remaining energy (I) is recorded. This operation, equivalent to a radiography, is repeated at regular angle intervals over 360 degrees around the samples, and provide a series of so-called projections. In the second phase, those projections are used to recover the 3D internal distribution of attenuation using an image reconstruction algorithm. The total attenuation, obtained in the first phase, depends on the linear attenuation coefficient of the material and its thickness, and is described by the Beer-Lambert law:

$$I = I_0 e^{-\mu x} \quad \textbf{(1)}$$

where I_0 is the X-ray intensity emitted by the X-ray source, μ is the linear attenuation coefficient of the material, x is the material thickness, and I is the resulting intensity. Pauwels (2017) defines μ as:

$$\mu = \frac{N_A}{A}\rho(\tau + \sigma) \quad \textbf{(2)}$$

where N_A is the Avogadro number, A is the atomic weight, and ρ is the density. τ and σ are respectively the photoelectric attenuation and Compton scattering probabilities, two X-ray attenuation phenomena, whose relative strength depends on the incident energy. Consequently, as mentioned above, X-ray attenuation depends on the density, the atomic composition and the porosity of the material.

A Siemens Somatom Definition AS+128 medical CT-scanner was used to produce stacks of 2D images that form 3D data. The acquisition and reconstruction parameters are reported in Table 1. For convenience, the medical CT-scanner software converts linear attenuation values into Hounsfield Unit (HU) where -1000 HU and 0 HU correspond to the linear attenuation of air and water, respectively.

Table 1. Parameters used for the CT-scanner acquisition and reconstruction.

Voltage (kV)	Exposure (mAs)	Spiral pitch factor	Kernel	Isotropic voxel size (mm)	HU range
140	350	0.55	H70h	0.1	-10240 to 30710

Since the positions of the TC profiles have been located using a permanent marker that cannot be detected on XCT images, a lead marker has been glued to the sample (after the measurements were taken with the TCS) to indicate the position of the first profile (Figure 1). The density contrast between rock and lead facilitates the location of the latter.

XCT images of 13 samples from the Bécancour area (Figure 2) reveal a variety of internal structural features. In sample 1, low-density heterogeneities, corresponding to darker areas, are randomly distributed throughout the volume. Sample 2 displays asymmetrically distributed granular particles. Planes with different orientations are observed in samples 3, 24, 25, 26, and 28, and a low level of heterogeneity is seen in samples 32 to 38, where dark circles, akin to pores, seem to be uniformly distributed. Sample 27 exhibits fractures, visible as vertical darker lines. The lead marker appears on the top side as a white box-shaped object because, in this case, it was aligned with the selected visualization plane during scanning.

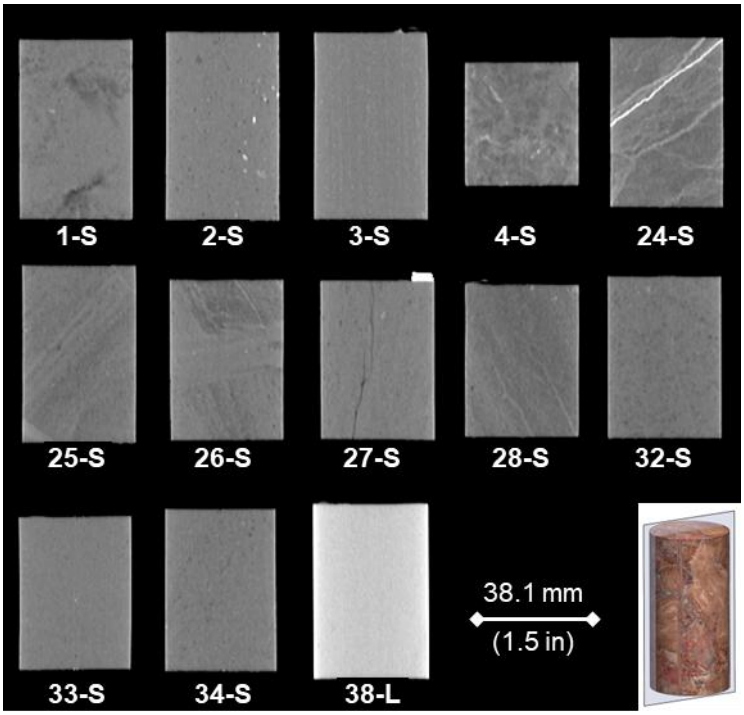


Figure 2. XCT images of the 13 Bécancour samples. The letter "L" and "S" identifies limestone and sandstone samples. These images correspond to 2D longitudinal planes, as illustrated in the bottom right corner.

The reference sample set, characterized by diverse lithologies and physical properties, also displays a range of internal structural features (Figure 3). Samples 39 and 48B display heterogeneously distributed high-density components, likely corresponding to heavy mineral phases, appearing as light regions in the XCT images.

No significant heterogeneity is observed in samples 40, 41B, 46A and 46B. Denser lines are present in samples 41A, 42A-B, 43A-B and 45A-B, indicating the presence of bedding. More complex structures can be seen in samples 44A, 47A-B and 49A, where sparsely distributed high-density features produce a mottled fabric throughout the volume.

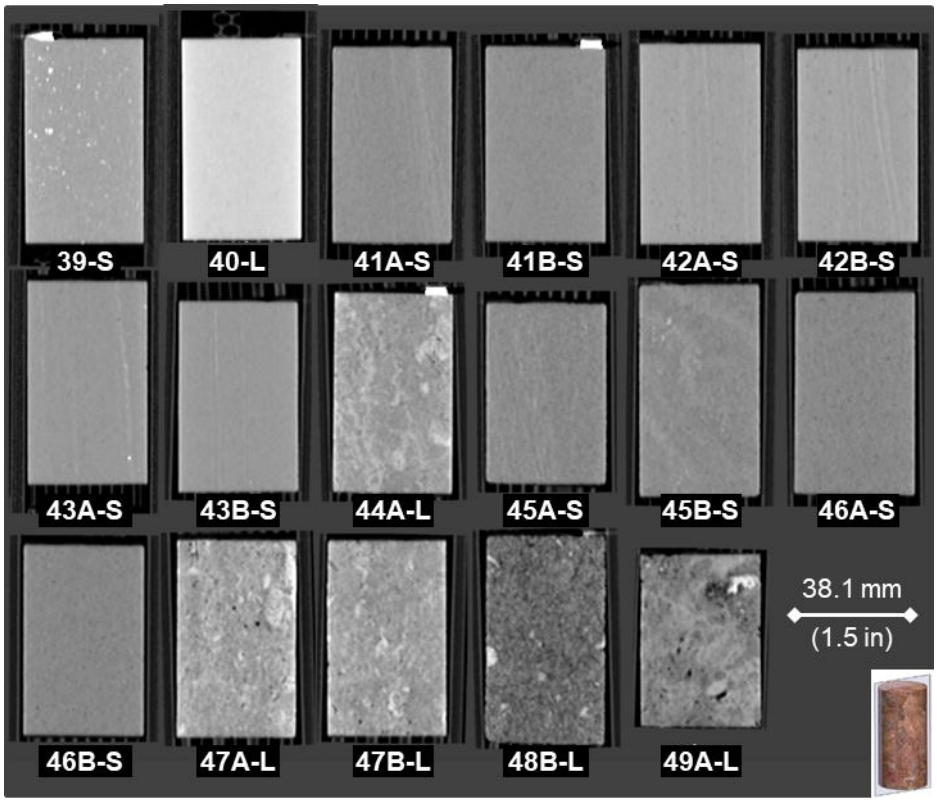


Figure 3. XCT images of reference samples. The letter "L" and "S" identifies limestone and sandstone samples. These images correspond to longitudinal planes, as illustrated at the bottom right corner.

2.4 Data processing

The algorithm was developed in Matlab to record and extract XCT-data at the same location where TCS measurements were made, and its steps are illustrated in Figure 4. The code has been named "Analysis of Thermal Conductivity and Hounsfield Unit data for Machine learning" or ATCHUM for short.

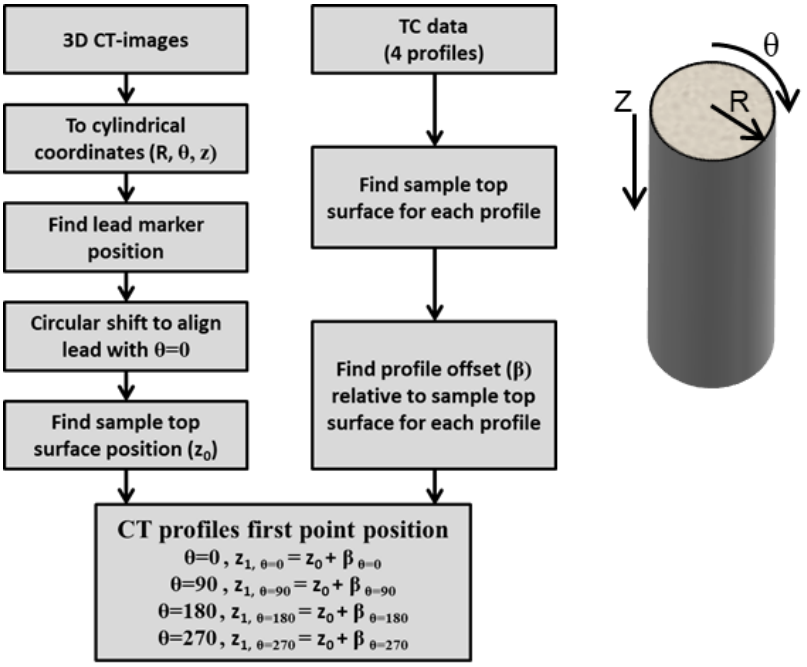


Figure 4. Steps of the algorithm developed for the alignment of X-ray imaging and thermal conductivity data.

The TCS output data include raw measurements and user-cropped profiles. To find the location of the sample top surface (Figure 5), the raw measurement of the temperature sensor is used. The position is obtained using the first derivative of the signal and the position of the positive peak (Figure 5). The starting position of the cropped profile is then translated with respect to the offset found and is now relative to the sample top surface. The same operations are applied to the XCT profiles to locate the top surface.

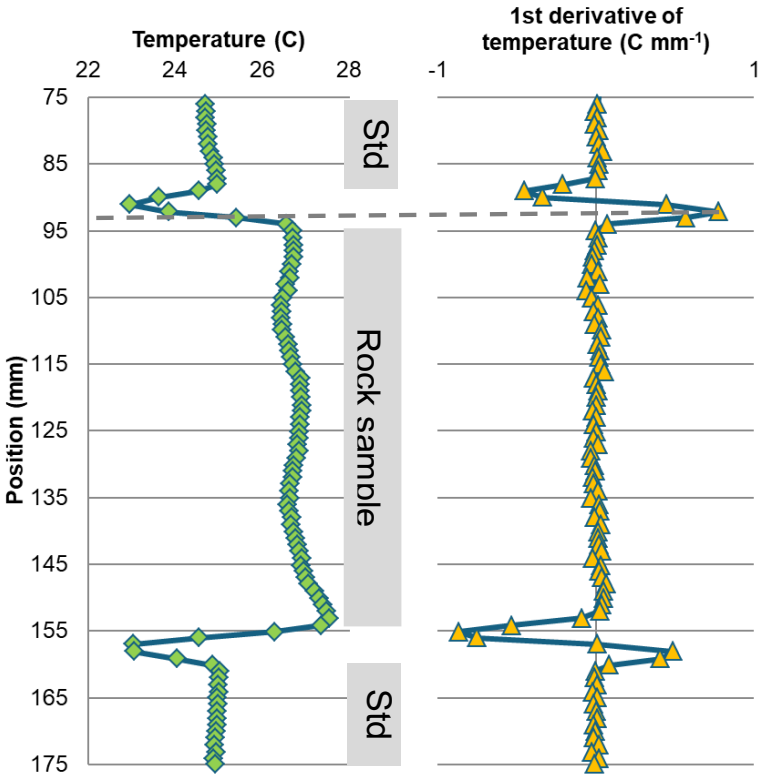


Figure 5. Determination of the location of the sample top surface position (horizontal dashed line) in TCS data profile

Once the location of the first TC data point is found in the XCT-data, the HU profile is extracted by picking the average XCT-data value within an ROI (region of interest) of 2 mm in θ and 1 mm in Z, at 1 mm intervals in the Z direction. The thickness or depth in R direction, used to evaluate the ROI corresponded to one image slice, equivalent to 0.1 mm.

To validate the algorithm, an evaluation of the registration accuracy was made by shifting XCT data origin by 1 mm from -2 mm to 2 mm for all profiles. The correlation and root mean square error (RMSE) were computed for each of the five cases.

3 RESULTS

3.1 ATCHUM code user interface

ATCHUM user interface is illustrated with data for sample 44A, a dolomite sample (Figure 6). The TC profiles are displayed at their corresponding positions over the unwrap XCT image (for a given radius in cylindrical coordinates). It is thus possible to observe the TC variation and density of local structures in HU. The registration process is fully automated, and the results are recorded in a tab-delimited file. This interface allows users to play with different features such as display brightness and contrast, and to select the range and positioning of the data they wish to view.

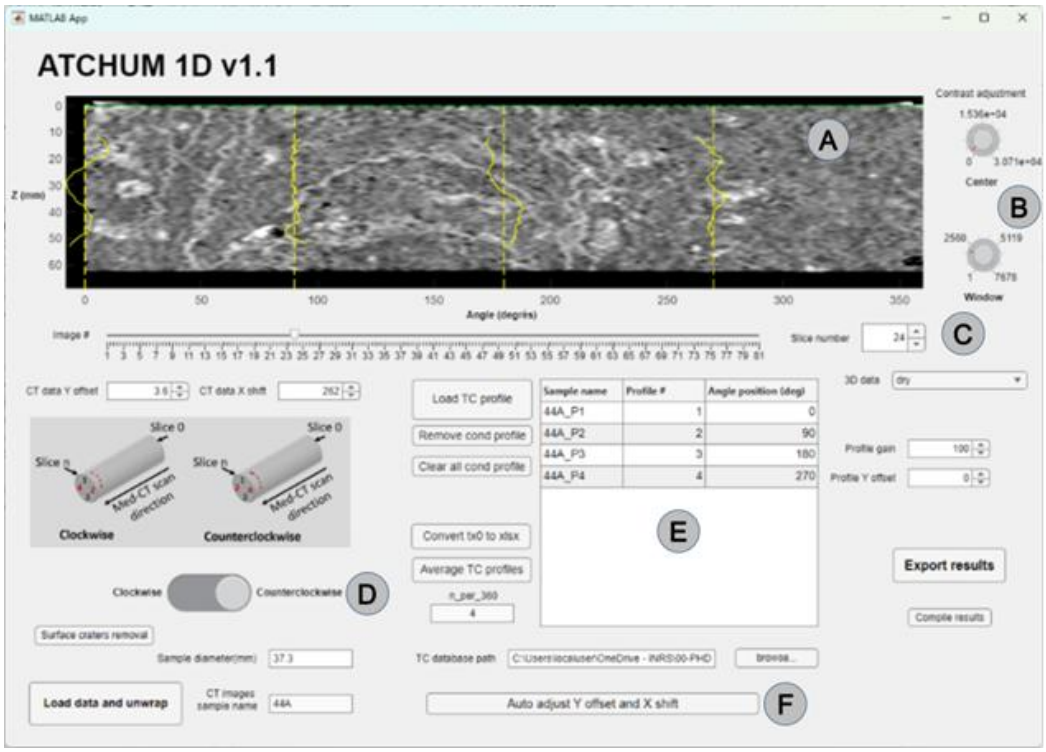


Figure 6. ATCHUM user interface. A: XCT unwrap image. B: Brightness and contrast display controls. C: Selector for the number of the unwrap slice. D: Profile numbering direction. E: TC data currently displayed in yellow on top of the unwrapped image. F: Automatic positioning function of the unwrapped image, moving the lead marker to the zero angle (θ) position.

3.2 Correlation of TC with XCT-data

A total of 3814 measurements, shown in Figure 7, were used to assess the TC and HU relationship. TC measurements range from 0.45 $Wm^{-1}K^{-1}$ to 5.23 $Wm^{-1}K^{-1}$. The correlation between the two parameters was found to be low when including the whole dataset (R^2=0.13). Considering the lithologies separately significantly increased the correlation: sandstone and limestone showed a coefficient of determination (R^2) of 0.43 and 0.91, with an RMSE of 0.7 and 0.2 $Wm^{-1}K^{-1}$, respectively.

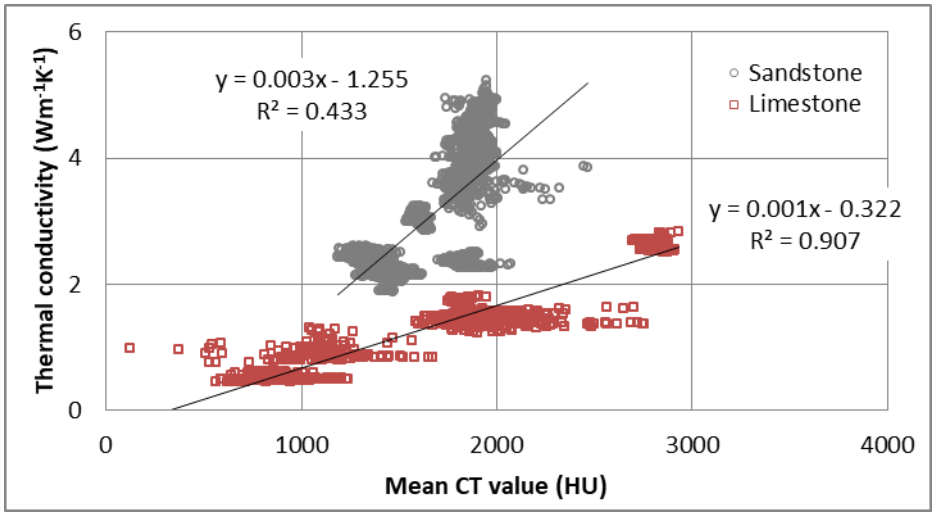


Figure 7. Correlation between XCT-data and TC.

In order to verify the influence of recording accuracy, correlation was evaluated for various shifted XCT data (from -2 to 2 mm). The results are presented in Table 2.

Table 2. Correlation and RMSE for the sandstone and limestone datasets

	Sandstone (23 samples)		Limestone (7 samples)	
XCT-data offset (mm)	Correlation (R^2)	RMSE ($Wm^{-1}K^{-1}$)	Correlation (R^2)	RMSE ($Wm^{-1}K^{-1}$)
-2	0.43	0.689	0.908	0.23
-1	0.432	0.689	0.907	0.231
0	0.434	0.688	0.907	0.231
1	0.432	0.690	0.906	0.233

The values obtained for limestones (7 samples) provide very good results, while the relationship for sandstones (23 samples) can be qualified as poor. The offsets do not seem to make any significant difference (<1%). Nevertheless, the null offset case has the highest correlation and lowest RMSE for sandstone, indicating that the first derivative approach is adequate.

3.3 3D representation of TC

Figure 8 shows the results of applying the linear regression model (Figure 7) to sample 44A and 49A XCT images, both of which are limestones. The 3D TC representation allows visualization of the internal rock heterogeneities. The two samples show a different spatial organisation of the high TC structures, visible as brighter gray level. Sample 49A has a markedly higher level of tortuosity than 44A, and both show scattered blobs.

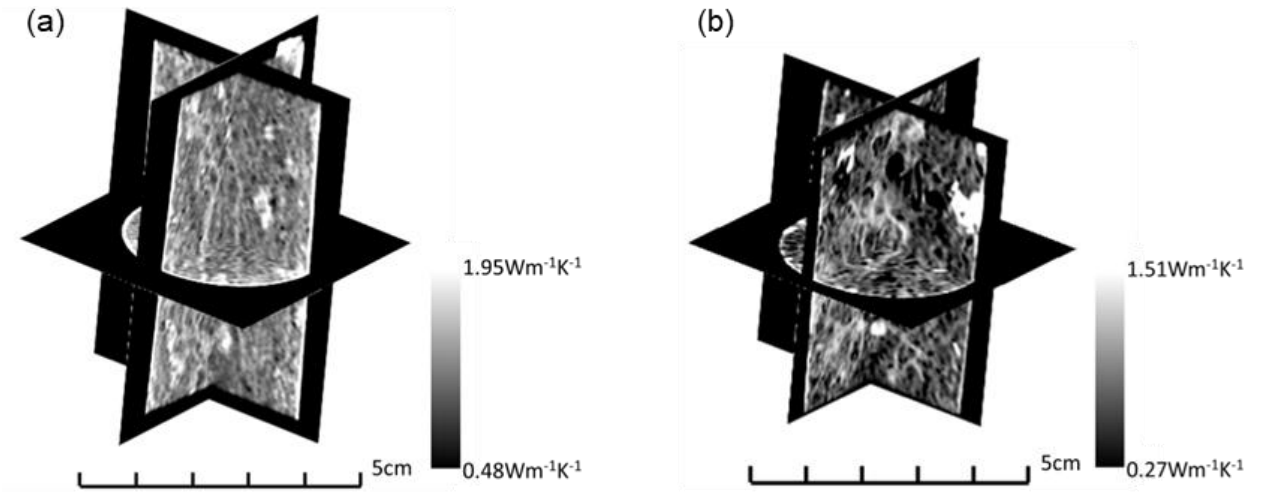


Figure 8. Examples of 3D representations of TC using three orthogonal planes for sample 44A (a) and 49A (b).

4 DISCUSSION

Taking into account the basic lithology (i.e., sandstone and limestone, without further characterization of their composition) considerably improved the relationship between TC and HU density compared to using the entire dataset. While a linear model produces a very good correlation for limestone (R^2>0.9), an exponential relationship would probably be more appropriate for sandstone. This significant difference in behavior may be attributed to the failure to account for TC anisotropy in the TCS measurements: bedding plane orientation, only present in sandstone in the current study, has an influence on the TCS data, while it does not affect XCT images. Moreover, even though HU values are influenced by porosity, density and chemical composition, the respective contributions of these three properties on the HU value are not distinguished, and they are inherently different between sandstones and limestones. A deeper investigation around the X-ray attenuation process is therefore required, in order to evaluate the influence of the geochemistry of the two lithologies on their respective attenuation spectra. To reduce the complexity of X-ray interaction with the material, a monochromatic X-ray source will be used, compared to a polychromatic one that was used for the current study.

Although this study assumed 1 cm as the heat penetration depth during a TCS measurement based on Popov's work (1997), this parameter is uncertain. Popov et al. (1983) reports, for a thickness of 5 mm, an error of less than 2% on TC for samples having a thermal diffusivity of 1 x 10^{-6} m^2s^{-1}, a value close to those of sandstones. Popov et al. (1999) also mention a depth of penetration of 2 to 3 cm or more for TC exceeding 6 $Wm^{-1}K^{-1}$. For this study, the first surface layer of material was used to extract HU values, corresponding to less than 1 mm, as it is considered to be the most representative of the TCS measurement, regardless of the TC value of the sample. Thus, the HU values do not include information on the deeper layers of material that may have influenced TC values. A better understanding of the depth of influence of the TCS measurement process would be necessary to establish the appropriate thickness of HU data to be extracted.

A few assumptions and issues related to the work presented here are worth highlighting. The conversion of HU to TC values in 3D is based on the assumption that the material at the surface is representative of the inner material, which makes the model directly applicable. However, it is not necessarily the case. Features such as fractures and bedding planes typically represent a small number of data points in the linear regression analysis and therefore have a higher level of error. This can be observed in Figure 7, where higher HU density values around a given group of data points are small in number. Consequently, such features do not carry a significant weight in the regression, even though they may have a significant impact on the behavior of the material. Finally, beam hardening, a well-known image X-ray artefact, can induce a tendency to underestimate HU values from the edge toward the center of the sample, biasing the model (linear in this case). Various algorithms for correcting beam hardening exist in the literature and will be carefully evaluated in order to make this surface-to-3D approach fully valid.

The 3D representation (Figure 8) illustrates the limitation of both 1D and 2D approaches: high internal TC structures can be present, unevenly distributed, tortuous, and difficult to capture adequately in all directions. 2D gridded characterisation, the finest approach as of today, constrains heat transfer simulation onto a plane, while the contribution of the third dimension, which could be significant in the presence of heterogeneities linked

to rapid shape changes, is neglected. The underestimation of TC from a TCS compared with values obtained with a divided bar device, as reported by Popov et al. (1999), may be due to the lack of representativeness of the sample as a whole resulting from 1D or 2D characterisation. This issue could be overcome using 3D TC data

5 CONCLUSION

Two models were developed for sandstone and limestone samples following data processing with the ATCHUM program to predict their TC using linear regression of XCT and TC values. A good level of correlation was obtained for limestone (R^2>0.9), while some additional aspects need to be considered for sandstone samples, as the correlation obtained was relatively low (R^2> 0.4). The application of these models to 3D HU data is straightforward. Although challenges remain to ensure the representativeness, and therefore the applicability of the model to the internal part of the sample, this study shows promising results towards 3D characterisation of TC. Combined with a 3D porosity map (Larmagnat et al., 2019) for a given rock, this work represents an important stepping stone towards a better understanding of the influence of rock heterogeneities on heat transfer, which has never been fully achieved.

Acknowledgements

We acknowledge the Geological Survey of Canada of Natural Resources Canada, the Fonds de Recherche du Québec – Nature et Technologies (FRQNT) and the Natural Sciences and Engineering Research Council of Canada (NSERC) for funding this study. We also recognize the contribution of Arnaud De Coninck and Philippe Letellier (Institut national de la recherche scientifique) for their meticulous work in sample preparation and data acquisition.

REFERENCES

Popov, Y., Pribnow, D., Sass, J., Williams, C. and Burkhardt, H.: Characterization of rock thermal conductivity by high-resolution optical scanning, *Geothermics*, **28**, (1999), 253-276

Jorand, R., Vogt, C., Marquart, G. and Clauser, C.: Effective thermal conductivity of heterogeneous rocks from laboratory experiments and numerical modeling, *Journal of Geophysical Research: Solid Earth*, **118**, (2013), 5225-5235

Popov, Y. A.: Optical scanning technology for nondestructive contactless measurements of thermal conductivity and diffusivity of solid matters., *Proceedings*, 4th World Conference on Experimental Heat Transfer, Fluid Mechanics and Thermodynamics, Brussels, Belgium, (1997)

Pauwels, E.: Optimal use of the polychromaticity in X-ray microtomography for dual energy methods and contrast agent imaging., *PhD thesis*, Ghent University, Ghent, Belgium (2017)

Popov, Y. A., Semenov, V. G., Korostelev, V. M. and Berezin, V. V.: Noncontact evaluation of thermal conductivity of rocks with the aid of a mobile heat source, *Earth Physics*, **19**, (1983), 563-567